

Interfacial Interaction in EVA-Carbon Nanotube and EVA-Clay Nanocomposites

HANS E. MILTNER,¹ SOPHIE PEETERBROECK,² PASCAL VIVILLE,³ PHILIPPE DUBOIS,² BRUNO VAN MELE¹

¹Vrije Universiteit Brussel (VUB), Physical Chemistry and Polymer Science (FYSC), Pleinlaan 2, B-1050 Brussels, Belgium

²Université de Mons-Hainaut, Service des Matériaux Polymères et Composites, Place du Parc 20, B-7000 Mons, Belgium

³Materia Nova ASBL, Service de Chimie des Matériaux Nouveaux, Avenue N. Copernic 1, B-7000 Mons, Belgium

Received 23 November 2006; accepted 2 March 2007

DOI: 10.1002/polb.21193

Published online in Wiley InterScience (www.interscience.wiley.com).

ABSTRACT: Proper filler-matrix compatibility is a key factor in view of obtaining nanocomposites with well-dispersed nanofillers displaying enhanced properties. In this respect, polymer-filler interaction can be improved by a proper combination of matrix and nanofiller polarities. This is explored for matrices ranging from nonpolar high density poly(ethylene) to ethylene-vinyl acetate (EVA) copolymers with varying vinyl acetate contents, in combination with several types of organoclay or carbon nanotubes. A novel *in situ* characterization methodology using modulated temperature differential scanning calorimetry is presented to evaluate the matrix-filler interaction. During quasi-isothermal crystallization of the matrix, an “excess” contribution is observed in the recorded heat capacity signal because of reversible melting and crystallization. Its magnitude considerably decreases upon addition of nanofiller in case of strong interfacial interaction, whereas the influence is moderate in case of a less interacting matrix-filler combination. It is suggested that the “excess heat capacity” can be used to quantify the segmental mobility of polymer chains in the vicinity of the nanofiller. Hence it provides valuable information on the strength of interaction, governed by the physical and chemical nature of matrix and filler. Heating experiments subsequent to quasi-isothermal crystallization point at a certain degree of molecular ordering, responsible for crystal nucleation in EVA copolymers. © 2007 Wiley Periodicals, Inc. *J Polym Sci Part B: Polym Phys* 45: 1291–1302, 2007

Keywords: crystallization; ethylene-vinyl acetate copolymer; interfaces; MTDSC; nanocomposites

INTRODUCTION

An everincreasing interest is currently being devoted to the study of nano-reinforced polymeric materials. The use of small amounts of nano-sized fillers such as organoclay or carbon nanotubes has resulted in the improvement of a wide span of material properties, thus outranging the unfilled matrix polymer. Improved barrier properties, superior mechanical properties, raised heat distortion

temperature, increased crystallization rate, flame retardant properties, and so forth have been reported.^{1–3} The origin of such superior properties, at filler loadings much smaller than in conventional microcomposites, is related to the small size and high aspect ratio of the nanoparticles, resulting in a tremendous amount of interphase material.

Getting the nanoparticles well-dispersed to exploit the high specific surface of the filler is therefore a prerequisite for achieving significant property enhancement. This is, however, also one of the challenging difficulties when preparing ther-

Correspondence to: B. V. Mele (E-mail: bvmele@vub.ac.be)

Journal of Polymer Science: Part B: Polymer Physics, Vol. 45, 1291–1302 (2007)
© 2007 Wiley Periodicals, Inc.

moplastic nanocomposites. In this respect, a key factor turned out to be the compatibility between polymer matrix and reinforcement. Effort has to be put into rendering matrix polymer and nanofiller compatible, for instance by modifying the surface characteristics of the filler particles. In case of clay filler, this is commonly achieved by exchanging cations with suitable organic surfactants. When carbon nanotubes are used, a small amount of specific functional groups (<1%) can, for instance, be grafted onto their surface by chemical treatment.^{4,5}

In the present work, nanocomposites based on semicrystalline ethylene-vinyl acetate copolymer (EVA) were studied. The influence of matrix polarity was investigated by considering matrix materials with different vinyl acetate content, and by comparison with nanocomposites based on nonpolar high density poly(ethylene) (HDPE). The evaluated nanofillers were organo-modified clays and various types of carbon nanotubes. Their polarities were fine-tuned by the choice of alkyl ammonium surfactant or by chemical surface treatment, respectively.

Modulated temperature differential scanning calorimetry (MTDSC) was employed for the investigation of the thermal properties of the nanocomposites, with a focus on the quasi-isothermal crystallization behavior of the matrix and its subsequent melting. The interplay between matrix and filler polarities, fine-tuned by the choice of matrix material and the type of nanofiller modification, allows the preparation of several systems with significant differences in thermal behavior. It is shown that the MTDSC technique can be used for quantifying the reduction in polymer segment mobility in the vicinity of the nanofiller and, thereto related, the strength of polymer-filler interaction. The employed methodology has been previously developed for poly(amide) 6/clay nanocomposites.^{6,7} In this article, the wide applicability of this approach is demonstrated and its sensitivity toward subtle changes in the material characteristics evidenced. The latter include slight modifications in the matrix and filler polarities, as well as the extension to carbon nanotube based composites.

EXPERIMENTAL

Materials

Commercial EVA copolymers with vinyl acetate (VA) contents ranging between 9.4 and 27 wt %

were obtained from Exxon Mobil: Escorene FL00209 (EVA(9.4), VA content 9.4 wt %, melt flow index (MFI, 190 °C/2.16 kg) 2.1 g/10 min), Escorene UL00112 (EVA(12), VA content 12 wt %, MFI 0.5 g/10 min), Escorene UL00119 (EVA(19), VA content 19 wt %, MFI 0.65 g/10 min), Escorene UL00328 (EVA(27), VA content 27 wt %, MFI 3 g/10 min).

HDPE was obtained from Dow Chemical (MFI 1.1 g/10 min).

Commercial organoclays were obtained from Southern Clay Products (USA): Cloisite[®] Na⁺, a natural Na⁺ montmorillonite; Cloisite[®] 20A, a montmorillonite modified by dimethyl bis(hydrogenated tallowalkyl) ammonium cations; Cloisite[®] 30B, a montmorillonite modified by methyl bis(2-hydroxyethyl) tallowalkyl ammonium cations.

The multiwalled carbon nanotubes (MWNTs) used in this work were supplied by the NMR Laboratory at the FUNDP (Belgium) and were produced by catalytic decomposition of acetylene on transition metal particles (Co, Fe) supported on Al₂O₃ (Nanocyl S.A., Belgium). Purified MWNTs were obtained after dissolution of the support in a boiling concentrated sodium hydroxide aqueous solution and dissolution of the catalyst in a concentrated hydrochloric acid aqueous solution. The MWNTs are characterized by an average length of about 15 μm, an average inner diameter of 5 nm, and an average outer diameter of 15 nm, corresponding to about 14–15 concentric layers.

Hydroxy-functionalization of the nanotubes is achieved by carboxylation using KMnO₄, followed by reduction using diisobutylaluminum hydride.⁸ Acetate-functionalization was obtained after reaction of the hydroxy-modified MWNTs with acetic anhydride. XPS analysis of the functionalized MWNTs reveals the presence of <1% of hydroxyl and acetate functions.

In addition, MWNTs were modified by metallocene-catalyzed HDPE polymerization filling technique. A homogeneous HDPE surface coating on the carbon nanotubes (~45 wt % HDPE) was achieved by *in situ* polymerization of ethylene, directly catalyzed from the nanotube surface treated by a highly active metallocene-based complex, allowing for the destructurement of the native nanotube bundles.⁹

Nanocomposite Preparation

Nanocomposites were prepared using the melt blending technique. Clay-based nanocomposites were compounded on an AGILA two-roll mill at

140 °C for EVA and 190 °C for HDPE, with a friction coefficient of 1.35 and a rate of 15 m/s. EVA/nanotube composites were prepared using a Brabender bench-scale internal mixer at 140 °C, for 12 min with a speed of 45 rpm.

Nanocomposite formulations are expressed by the weight fraction of nanofiller (expressed as the inorganic content in case of organomodified clays) present in the sample, as determined by thermogravimetric analysis.

Characterization Techniques

Both nonisothermal and quasi-isothermal MTDSC measurements were performed under helium flow (25 mL/min) using TA Instruments Q1000 equipment with T-zero™ DSC-technology and with an RCS cooling accessory. Temperature and enthalpy calibration were performed using an indium standard. DSC data are expressed as specific heat capacities ($J/g^{\circ}C$) or specific heat flows (W/g) on polymer basis. All experiments were conducted on samples preliminary melted at sufficiently high temperature to fully erase their thermomechanical history.

Test specimens for Atomic force microscopy (AFM) studies were prepared with a LEICA cryomicrotome equipped with a diamond knife and maintained at $-80^{\circ}C$. The AFM images were recorded in tapping mode in ambient atmosphere at room temperature with a Nanoscope IIIa microscope (Veeco Inst., Santa Barbara, CA). The probes were commercially available silicon tips with a spring constant of 24–52 N/m, a resonance frequency in the 264–339 kHz range, and a typical radius of curvature in the 10–15 nm range. Images obtained in phase detection were recorded with the highest sampling resolution available, that is 512×512 data points.

RESULTS AND DISCUSSION

Nanocomposite Morphology

Prior to characterization by advanced thermal analysis methods, the morphology of the prepared nanomaterials was assessed. AFM was used to evaluate the dispersion quality of the nanofillers within the matrix. Figure 1 shows the morphologies obtained for different EVA(27) nanocomposites.

For the nanocomposite based on Cloisite® 30B [Fig. 1(a)], a large extent of exfoliation is obtained.

Journal of Polymer Science: Part B: Polymer Physics
DOI 10.1002/polb

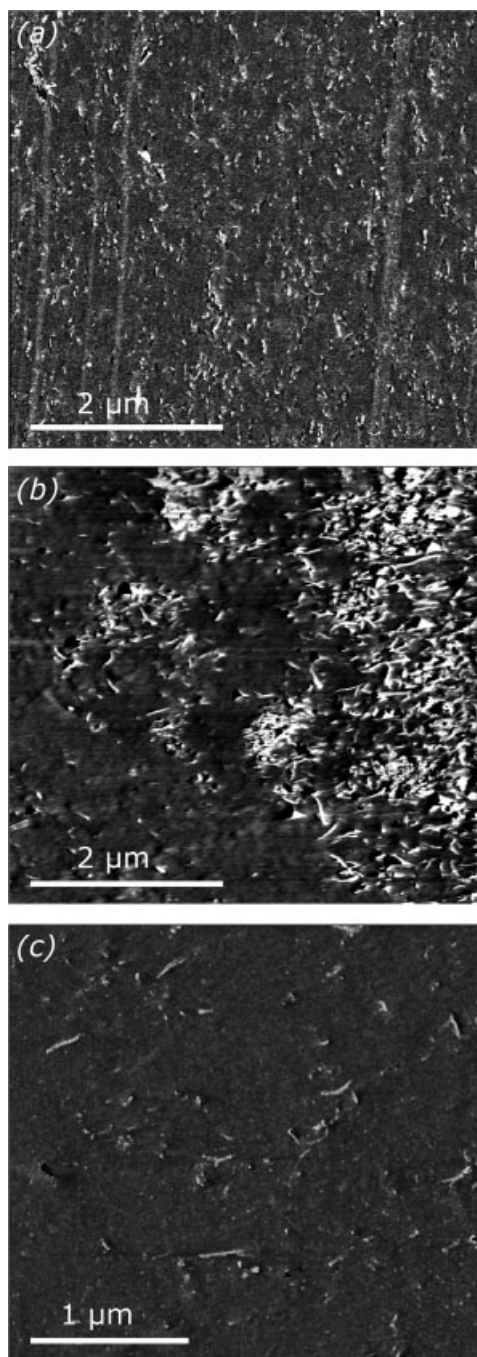


Figure 1. AFM images recorded in tapping mode for EVA(27)-based nanocomposites containing 3 wt % of Cloisite® 30B (a), 3 wt % of multi-walled carbon nanotubes (b) and 3 wt % of HDPE-coated multi-walled nanotubes (c).

Very small stacks (2–4 nanoplatelets) as well as individual clay nanoplatelets can be observed, which are well-dispersed throughout the matrix.

Figure 1(b) shows the morphology of a nanocomposite containing untreated MWNTs. Micron-scale

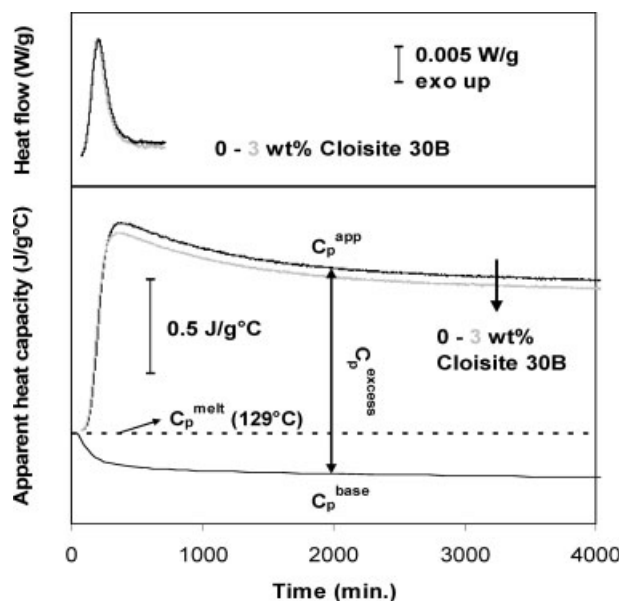


Figure 2. MTDSC heat flow (top) and heat capacity (bottom) signals recorded during quasi-isothermal crystallization of HDPE and a nanocomposite containing 3 wt % of Cloisite[®] 30B (modulation conditions 129 °C ± 0.5 °C/60 s).

bundles of nanotubes are observed, along with a few isolated MWNTs. A homogeneous dispersion throughout the matrix could not be achieved. The morphology of the nanocomposite based on HDPE-coated MWNTs is shown in Figure 1(c). The AFM phase image only shows isolated MWNTs homogeneously dispersed throughout the matrix, without any remaining agglomerates.

Quasi-Isothermal Crystallization by MTDSC

High Density Poly(ethylene)

MTDSC Methodology. In the study of polymer materials by means of MTDSC, the kinetics of thermal processes, depending on time and absolute temperature, often appear in the “nonreversing” heat flow, while the (specific) heat capacity is found in the “reversing” heat flow. The former signal equals the total heat flow (the running average of the modulated signal) minus the “reversing” heat flow. A complete description of the extraction of the heat capacity and other MTDSC signals can be found in literature.^{10,11}

The straightforward distinction of heat capacity and thermal transformations in separate MTDSC signals is no longer valid in case of polymer melting or phase separation in polymer blends and sol-

utions. Heat effects coupled with melting/crystallization^{12–14} or mixing/demixing^{15–19} can occur during one modulation cycle and thus contribute to the heat capacity signal. Hence, the latter is termed “apparent” heat capacity, C_p^{app} , to distinguish it from the baseline heat capacity based on thermodynamics, C_p^{base} , which is temperature-dependent. The so-called “excess” contribution, C_p^{excess} , is temperature and time-dependent and changes with the progress of the transformation:

$$C_p^{app} = C_p^{base} + C_p^{excess}$$

During quasi-isothermal crystallization a decrease is expected in the heat capacity signal, to an extent reflecting the attained degree of crystallinity (C_p^{base}). In certain cases, however, the observed heat capacity signal C_p^{app} contains an excess contribution C_p^{excess} , which originates from the heat effects associated with melting and crystallization of a polymer fraction on the timescale of the temperature modulation. An example of such behavior showing the used terminology is depicted in Figure 2 for the quasi-isothermal crystallization of HDPE.

In the novel approach presented in this work, the “excess contribution” to the heat capacity during quasi-isothermal crystallization is related to polymer-filler interaction and to segmental mobility. This methodology, which allows the *in situ* monitoring of the crystallization process, has been first introduced for poly(amide) 6/clay nanocomposites and can be extended to any composite material with a semicrystalline matrix.^{6,7} In the present article, the origin, magnitude, and time-dependency of C_p^{excess} for the crystallizing nanocomposites will be related to melting/crystallization processes in the interphase region between polymeric matrix and reinforcement. It is shown that these processes are governed by the polymer-filler interfacial interaction, providing new insight into the physical/chemical processes occurring at the nanoscale and which are the basis for the highly improved material properties in polymer nanocomposites.

Effect of Clay Loading. The MTDSC signals recorded during quasi-isothermal crystallization of HDPE and a clay nanocomposite containing 3 wt % of Cloisite[®] 30B are shown in Figure 2. At 129 °C, the crystallization process is characterized by an induction period reflecting the crystal nucleation, followed by the crystal growth observed as an exothermic heat flow. Under the chosen modu-

lation conditions of ± 0.5 °C/60 s, a considerable excess contribution is observed in the heat capacity signal (as calculated with respect to the baseline level, which depends on the degree of crystallinity developed in the sample²⁰). On the timescale of the imposed temperature modulation, a portion of the material is able to undergo reversible melting and crystallization. The heat effects associated with this “fast” process appear in the apparent heat capacity signal. Simultaneously, a “slow” long-term evolution is observed even long after the heat flow signal has reached its baseline level, reflecting the underlying process of crystallization which cannot be monitored *in situ* and in real time using the heat flow signal.

As observed in Figure 2, the presence of clay only shows limited effect on C_p^{excess} . Only a slight reduction is observed when comparing the levels of C_p^{app} for unfilled HDPE and for HDPE filled with 3 wt % of Cloisite[®] 30B with respect to their calculated baseline C_p^{base} . This signifies that the presence of organoclay does not influence the “fast” reversible melting and crystallization to a large extent, which is not unexpected in view of the lack of strong interactions between the nonpolar polyolefinic matrix and organoclay.²¹

Ethylene-Vinyl Acetate Copolymer

It is well-established that fine-tuning the polarities of matrix and filler is crucial to achieve good compatibility.^{1,22} Polarity can be introduced into poly(ethylene) by randomly incorporating vinyl acetate units, which moreover allows to fine-tune the physical and chemical properties of the material.²³ Nanocomposites based on EVA copolymer constitute an interesting model system in that the polarity of the matrix can be easily modified by the choice of the vinyl acetate content.^{24–26} It has been demonstrated that increasing the polarity of the matrix, that is the VA content, improves its affinity for organoclay and leads to increased interlayer distances in the corresponding nanocomposites.^{25,27}

Samples of EVA(19) and EVA(27), loaded with different types and amounts of clay or carbon nanotubes, have been quasi-isothermally crystallized at 78 and 67 °C, respectively, with an imposed temperature modulation of ± 0.5 °C/60 s. The evolution of the heat capacity signal is used for monitoring the ongoing process. As for the previously described HDPE-based nanocomposites, crystallization of EVA(19) under the chosen conditions results in the presence of an excess contribu-

tion C_p^{excess} superimposed onto the baseline heat capacity C_p^{base} (Fig. 3).

Influence of Clay Content. As can be observed in Figure 3, the magnitude of C_p^{excess} during quasi-isothermal crystallization of EVA(19) decreases upon addition of Cloisite[®] 30B nanoclay, to an extent depending on the loading. Comparable observations were reported for poly(amide) 6/clay nanocomposites.^{6,7} For the latter systems, a similar decrease in C_p^{excess} was observed with increasing filler loading, which was interpreted in terms of a decrease in polymer chain segment mobility because of strong interaction with the polar filler. Because of this decreased segmental mobility, part of the matrix material located in the vicinity of the filler is no longer able to participate in the fast process of reversible melting and crystallization, that is, insufficient time for reversible melting and crystallization is provided to the polymer under the chosen temperature modulation conditions. Therefore, less excess heat of melting and crystallization contributes to C_p^{app} . Similarly, strong interaction is anticipated between polar organoclay (Cloisite[®] 30B) and acetate moieties in EVA-based nanocomposites, resulting in a decreased mobility in the vicinity of the platelets. This is supported by the comparison between the magnitudes of C_p^{excess} shown in Figures 2 and 3, evidencing that the organo-modified clay restricts the chain segment mobility of the EVA(19) matrix to a much larger extent than in the case of nonpolar HDPE.

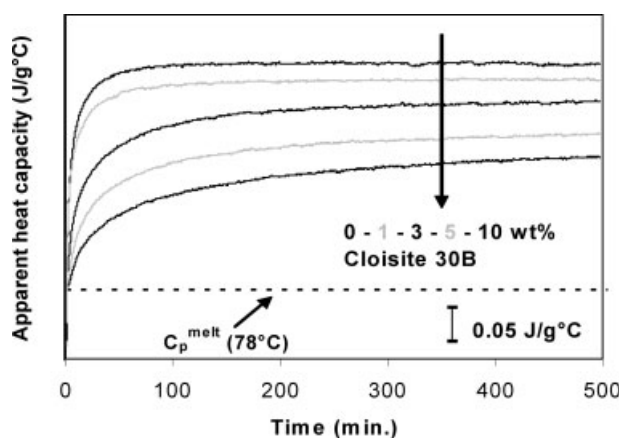


Figure 3. Apparent heat capacity recorded during quasi-isothermal crystallization of EVA(19) and its nanocomposites containing various loadings of Cloisite[®] 30B (indicated by arrow; modulation conditions 78 °C \pm 0.5 °C/60 s).

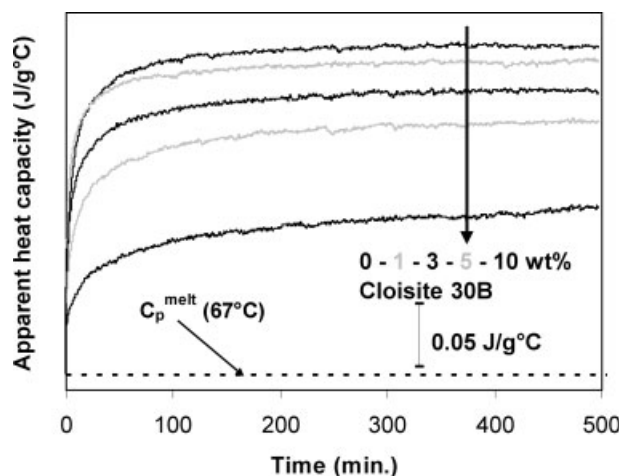


Figure 4. Apparent heat capacity recorded during quasi-isothermal crystallization of EVA(27) and its nanocomposites containing various loadings of Cloisite[®] 30B (indicated by arrow; modulation conditions 67 °C ± 0.5 °C/60 s).

Influence of Vinyl Acetate Content. The effect of matrix polarity was further investigated by considering EVA-based nanocomposites with different vinyl acetate contents. The quasi-isothermal crystallization behavior of the unfilled matrices (e.g., EVA(27)), is comparable to that of EVA(19) previously shown in Figure 3. Similarly, the magnitude of C_p^{excess} decreases upon addition of polar Cloisite[®] 30B, to an extent depending on its loading (Fig. 4).

To assess the influence of matrix polarity for nanocomposites based on a polar organoclay, C_p^{excess} was determined for the neat matrix material and for its nanocomposite containing 3 wt % of Cloisite[®] 30B. It is anticipated that the lower the VA content, the weaker the interaction with the filler and the lesser the reduction in segmental mobility. This should be reflected in the magnitudes of C_p^{excess} for the different systems, with a proportionally lower C_p^{excess} for EVA-based nanocomposites with high VA content. As C_p^{excess} also depends on the underlying isothermal temperature, that is the supercooling for each specific system, C_p^{excess} for the nanocomposites was expressed as a relative percentage of C_p^{excess} corresponding to the unfilled EVA, and the relative decrease in C_p^{excess} was taken as a measure for the strength of polymer-filler interaction. Note that, because of the absence of reliable baseline heat capacity data for EVA, C_p^{excess} was estimated with respect to the C_p value of the EVA melt at the corresponding quasi-isothermal crystallization temperature, as determined from nonisothermal MTDSC experiments.

Since the degree of crystallinity of the matrix remains nearly unchanged upon addition of nanofiller, it is reasonable to assume equal baselines for the unfilled and filled matrix.

For all evaluated matrices, the addition of nanoclay tends to decrease the magnitude of C_p^{excess} (i.e., “Relative C_p^{excess} ” < 100%), as plotted in Figure 5 against vinyl acetate content. Compared to HDPE, the relative reduction in C_p^{excess} is stronger when polarity is introduced into the matrix material, which is in line with the assumed stronger interaction with the nanoclay, more strongly affecting the chain segment mobility of the matrix polymer, hence also C_p^{excess} . However, the trendlines in Figure 5 show that this relative decrease in C_p^{excess} levels off at higher VA contents, suggesting that further introducing polarity is no longer beneficial in view of achieving stronger matrix-filler interaction. Earlier studies evaluating the increase in organoclay gallery spacing upon increasing the vinyl acetate content led to similar conclusions. A progressive increase in the gallery spacing was reported for VA contents increasing up to 12 wt %, but it remained constant upon further increase.²⁷ An explanation might be the fact that the viscosity of the polymer melt decreases with increasing vinyl acetate content. The shear stresses during melt processing of the nanocomposites are therefore more limited and the quality of the achieved organoclay dispersion is less, hence limiting the effect of clay on the segmental mobility of the matrix polymer because of the limited available interface surface with the nanofiller. Note that a changing degree of crystallinity of the matrix with increasing VA content cannot be held

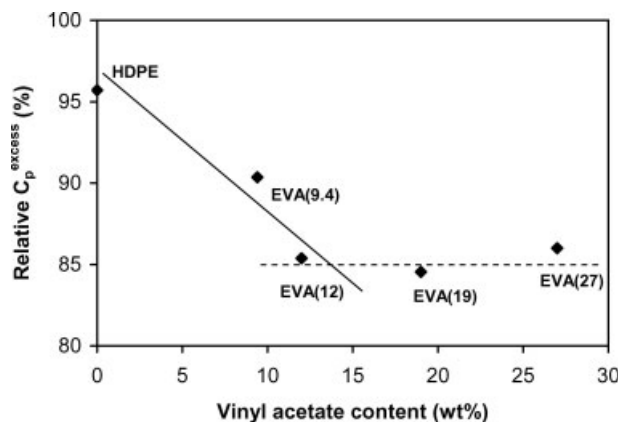


Figure 5. Relative excess heat capacity of nanocomposites containing 3 wt % of Cloisite[®] 30B as a function of the vinyl acetate content of the matrix (solid and dashed trendlines: see discussion in text).

responsible for the observed trend in Figure 5, as this aspect is already taken into account by considering relative values of C_p^{excess} .

Importance of Interaction Type: Use of Different Nanofillers

The effect of polymer-filler interaction type was investigated by considering EVA(27) as the matrix material, in combination with several types of polar and nonpolar filler particles, that is different organoclays and various types of MWNTs. The chemistry of the nanofiller is expected to strongly influence the type of interaction it undergoes with the polymer matrix, hence alter its segmental mobility and, for instance, modify its quasi-isothermal crystallization behavior. The applicability of MTDSC to obtain insight into the dynamics of physical and chemical processes occurring in nanostructured materials is demonstrated in the subsequent paragraphs.

Influence of Organoclay Type. It was argued that organoclay is preferentially located in the amorphous portion of the EVA matrix.^{28,29} This is mainly related to the molecular and crystalline structure of EVA. Several studies demonstrated that the EVA chain structure essentially consists of isolated vinyl acetate units randomly distributed among longer ethylene sequences.^{23,30} Crystallization only occurs in the ethylene segments, with the vinyl acetate units expelled to the amorphous fraction. However, in view of the polarity of organoclay, it is assumed that interaction mainly occurs with the vinyl acetate units, which are located in the amorphous part of the semicrystalline polymer. Nevertheless, quasi-isothermal crystallization experiments did reveal a significant influence of the nanofiller on the crystallization behavior, therefore suggesting that the crystallization of ethylene segments is affected by the interaction of organoclay with nearby vinyl acetate units. Henceforth, it is concluded that interfacial interaction essentially concerns the amorphous polymer fraction, but that it also affects the mobility of the crystallizable ethylene sequences located in its vicinity. It is the latter mobility restriction that can be evidenced by the diminution in C_p^{excess} during quasi-isothermal crystallization.

The situation is different when considering nanocomposites with less polar organoclay, that is Cloisite[®] 20A. As can be observed in Figure 6, the magnitude of C_p^{excess} is decreased to a much stronger extent upon addition of 3 wt % of Cloisite[®] 20A

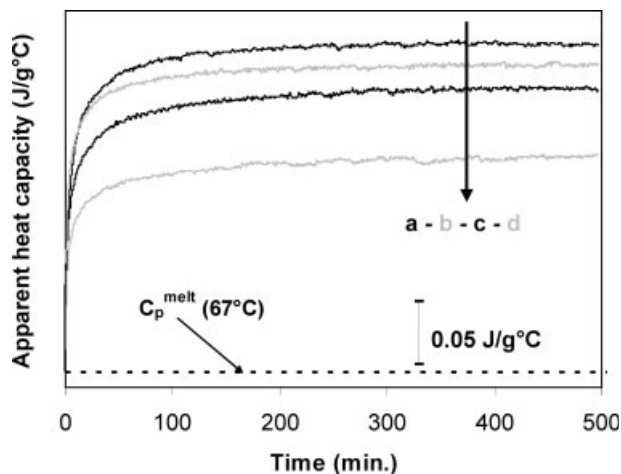


Figure 6. Apparent heat capacity recorded during quasi-isothermal crystallization of EVA(27) and its nanocomposites containing different types of clay filler: unfilled EVA(27) (a), 3 wt % Cloisite[®] Na⁺ (b), 3 wt % Cloisite[®] 30B (c), 3 wt % Cloisite[®] 20A (d) (sequence indicated by arrow; modulation conditions 67 °C ± 0.5 °C/60 s).

than it is the case for 3 wt % of Cloisite[®] 30B, because of a different type of interaction occurring with the nonpolar Cloisite[®] 20A. This clay contains long aliphatic surfactant molecules, likely to interact with the ethylene segments by a Van der Waals type interaction rather than by polar interaction with vinyl acetate units (which are, however, still able to interact with the polar clay surface). Therefore in this case the interaction directly affects the crystallizable EVA fraction, hence reducing C_p^{excess} to a larger extent. This is also reflected in the lower attained degree of crystallinity in nanocomposites based on Cloisite[®] 20A, as will be shown further (Fig. 9).

Finally it is worth noting that when untreated clay is used, that is Cloisite[®] Na⁺, the effect on C_p^{excess} is very limited (Fig. 6). This is due to the fact that this clay is poorly dispersed in the EVA matrix, hence limiting the surface available for interfacial interaction and related mobility restriction.

Influence of Carbon Nanotube Type. As an extension to the applied methodology, and to further investigate the importance of interaction type, similar quasi-isothermal crystallization experiments have been conducted on EVA(27) filled with various types of carbon nanotubes (Fig. 7). Because of the lack of strong interactions between the polar matrix and the untreated carbon nanotube surface, a much lesser reduction in C_p^{excess} , if

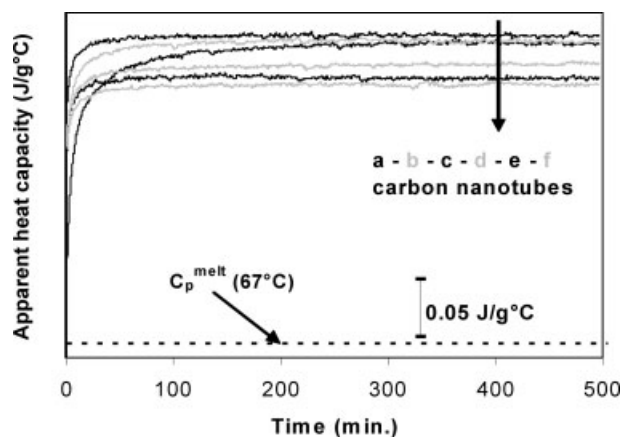


Figure 7. Apparent heat capacity recorded during quasi-isothermal crystallization of EVA(27) and its nanocomposites containing different types of carbon nanotubes: 5 wt % multi-walled nanotubes (a), 1 wt % multi-walled nanotubes (b), unfilled EVA(27) (c), 3 wt % HDPE-coated nanotubes (d), 3 wt % acetate-functionalized nanotubes (e), 3 wt % hydroxy-functionalized nanotubes (f) (sequence indicated by arrow; modulation conditions $67^{\circ}\text{C} \pm 0.5^{\circ}\text{C}/60\text{ s}$).

any, is anticipated for filled EVA(27) as compared to the unfilled matrix material. This is experimentally confirmed since C_p^{excess} remains constant when untreated carbon nanotubes are added, irrespective of the loading (Fig. 7). However, a decrease in C_p^{excess} is observed upon addition of chemically functionalized carbon nanotubes bearing acetate or hydroxy moieties at their surface, capable of polar interaction with the vinyl acetate units. As in the case of clay-filled EVA(27), this is a direct indication of polymer-filler interaction and decreased polymer segment mobility. The effect is lesser, however, as compared to the clay-filled systems at similar loading, which is due to the limited degree of nanotube functionalization (note that Figs. 4 and 7 are drawn on the same scale).

Figure 7 also shows the apparent heat capacity for nanocomposites based on carbon nanotubes previously coated with a thin layer of HDPE, allowing for a better dispersion throughout the matrix and increasing the surface available for interfacial interaction.⁹ It can be observed that in this case C_p^{excess} is also reduced, to an extent nearly comparable to when polar functionalized carbon nanotubes are used. In this case, as for Cloisite[®] 20A clay, the interaction with the EVA matrix primarily concerns the crystallizable ethylene sequences which undergo Van der Waals type interaction with the HDPE coating of the nanotubes. As discussed further (Fig. 9), this is also

reflected in the lower degree of crystallinity of the matrix.

It is worth mentioning that in the nanotube-filled systems the equilibrium value of C_p^{app} is attained much faster than in the case of the unfilled matrix (compare trace c to traces a, b and d–f in Fig. 7), suggesting that crystal nucleation occurs to a significant extent.³¹ In addition, a slight increase in C_p^{excess} is observed at higher nanotube loadings, which might be related to the presence of smaller crystallites as a result of the nucleating effect. The higher specific surface of those crystallites provides considerably more crystal-melt interface for reversible melting and crystallization, hence leading to an increased magnitude of C_p^{excess} .

The results discussed thus far point out the potential use of MTDSC for assessing the strength of interfacial polymer-filler interaction in nanocomposites with a semicrystalline matrix. Moreover, it provides valuable insight into the nature of the different interaction types, and how these affect the segmental mobility and crystallization behavior of the ethylene sequences. Finally, the presented MTDSC methodology might provide an estimate for the achieved degree of nanofiller dispersion, since the decrease in segmental mobility is directly related to the available amount of polymer-filler interface.

Melting Behavior After Quasi-Isothermal Crystallization

Unlike for the systems based on poly(amide) 6^{6,7} or poly(ethylene) (see above discussion), the absence of an induction period—even in case of the unfilled matrix—is indicative for a very fast nucleation process during EVA crystallization. This was observed at any of the explored quasi-isothermal crystallization temperatures, for all EVA types investigated (Figs. 3, 4, 6, and 7). Conditions for which the crystallization does exhibit an induction period could not be found. A possible explanation is the presence of locally structured zones in the melt, which consist of aggregated vinyl acetate units molecularly segregated from the ethylene sequences. This is not unlikely in view of the reported immiscibility of poly(ethylene) and EVA copolymer.^{32–34}

Influence of Crystallization Time

To gain further insight into the peculiar crystallization behavior of EVA and its nanocomposites,

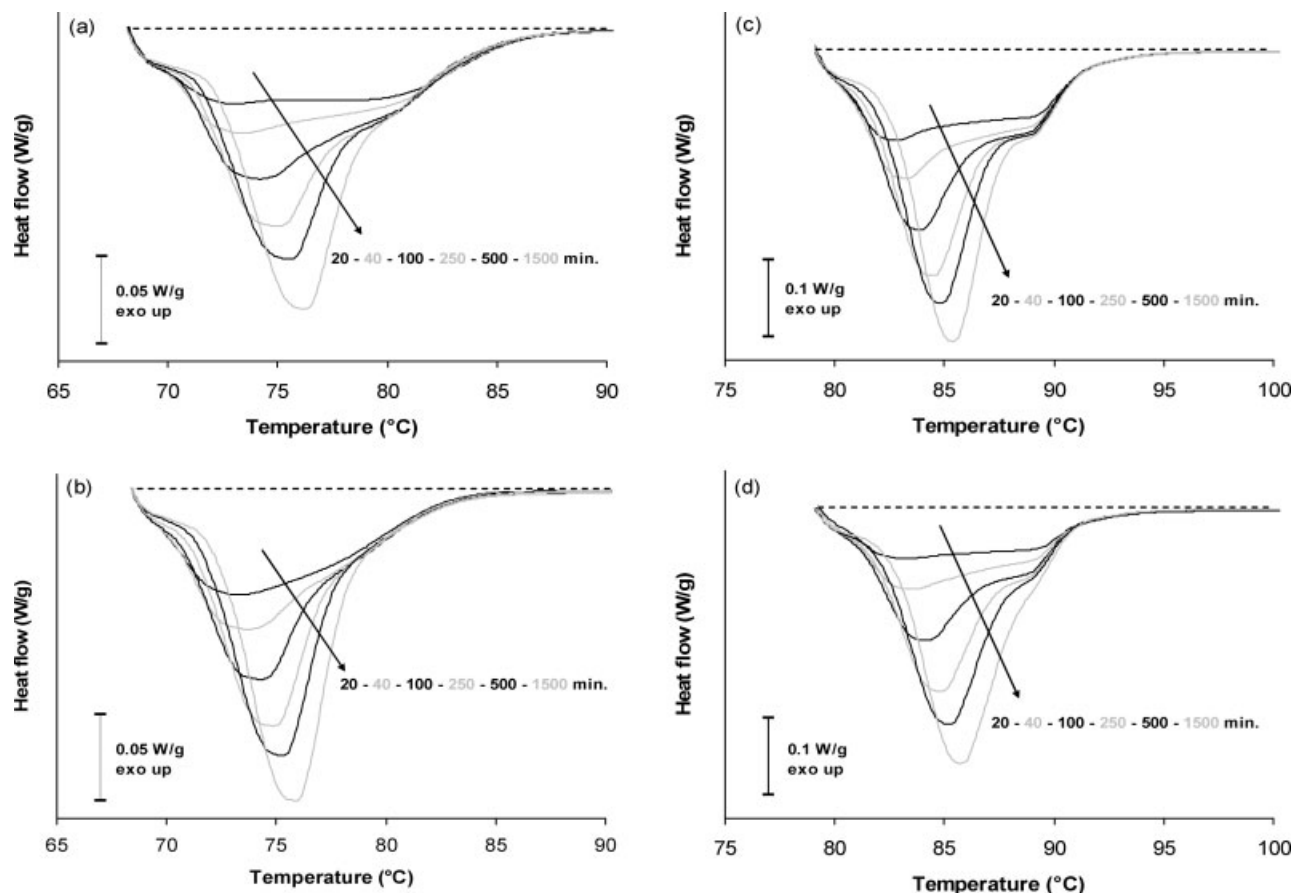


Figure 8. Heat flow signal recorded during heating experiments subsequent to various times of quasi-isothermal crystallization: unfilled EVA(27) (a), EVA(27) + 3 wt % HDPE-coated nanotubes (b), unfilled EVA(19) (c), EVA(19) + 3 wt % Cloisite[®] 30B (d) (crystallization times indicated by arrow; heating experiments at 5 °C/min. using conventional DSC).

the melting traces subsequent to increasing quasi-isothermal crystallization times were recorded for different samples of EVA(27) and EVA(19) (Fig. 8). It can be observed that the degree of crystallinity strongly depends on the quasi-isothermal crystallization time. Regarding the shape of the melting transition, several observations can be drawn. Melting of a crystalline fraction already sets in immediately above the isothermal crystallization temperature, as observed as a shoulder to the endothermic heat flow signal corresponding to the melting of the main crystalline fraction. This indicates the presence of a fraction crystallized almost without supercooling. This fraction is formed in the early stages of the crystallization process, as attested by the fact that it already appears after short crystallization times. Hence, the observed shoulder cannot be attributed to the melting of secondary crystals of lesser perfection, formed in a later stage in between the more perfect crystals. It

is therefore suggested that this crystal fraction originates from a nucleation process due to a certain degree of ordering in the melt, which might be related to local aggregation of vinyl acetate units, molecularly phase-separated from the ethylene-rich fraction. Its importance is more prominent in the melting traces of samples based on EVA(27) compared to those based on EVA(19), which is in line with the higher vinyl acetate content. The melting temperature of this fraction is lower than for the bulk crystalline fraction, indicating a lower degree of perfection. This is in agreement with the fact that these low-melting crystals contain the ethylene sequences located close to the vinyl acetate moieties, hence experiencing the largest influence of the noncrystallizable constituents.

An additional feature can be observed in the shape of the melting transition. In addition to the shoulder at the low-temperature end of the transition, a more prominent tail also appears at its

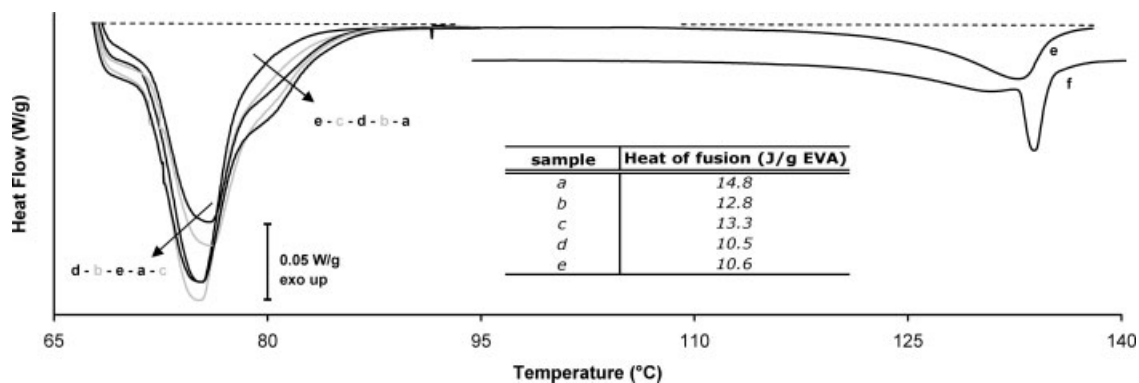


Figure 9. Heat flow signal recorded during heating experiments subsequent to quasi-isothermal crystallization of EVA(27) and its nanocomposites (500 min. at $67\text{ }^{\circ}\text{C} \pm 0.5\text{ }^{\circ}\text{C}/60\text{ s}$): unfilled EVA(27) (a), 3 wt % Cloisite[®] 30B (b), 3 wt % multi-walled carbon nanotubes (c), 3 wt % Cloisite[®] 20A (d), 3 wt % HDPE-coated nanotubes (e). Trace (f) shows the effect of annealing at $130\text{ }^{\circ}\text{C}$ for 10 min.; the inset table shows the heat of fusion for all samples (heating experiments at $5\text{ }^{\circ}\text{C}/\text{min.}$ using conventional DSC).

high-temperature end. This suggests the presence of a crystalline fraction of higher perfection, already present after short crystallization times as well. This tail can be attributed to the most perfect crystalline fraction in the EVA, that is the longest ethylene sequences which experience the least influence from the vinyl acetate units.^{23,35}

Influence of Nanofiller Type

When comparing the melting traces of the unfilled EVA(27) matrix and different nanocomposites, it appears that the shape of the transition depends on the system investigated (Figs. 8 and 9). The high-temperature tail is not equally apparent in all samples, that is its importance is negligible in the nanocomposites based on carbon nanotubes, suggesting that the latter more strongly affect the crystal morphology of the matrix. It is assumed that the growth of crystals of higher perfection is suppressed by the strong nucleating effect of the carbon nanotubes, promoting fast growth of crystals of less perfection with a slightly lower melting temperature. Also note in this respect that the low-temperature shoulder is not suppressed by the addition of nanofillers, confirming that it is an intrinsic characteristic of the matrix polymer.

With respect to the degree of crystallinity attained after quasi-isothermal crystallization (500 min at $67\text{ }^{\circ}\text{C}$), the values of the heat of fusion are reported in Figure 9 for EVA(27) samples containing 3 wt % of nanofiller. It can be observed that the degree of crystallinity is almost unaffected by the presence of untreated carbon nanotubes or

Cloisite[®] 30B organoclay. This is not unexpected in view of the type of interaction these nanofillers undergo with the matrix. In case of untreated carbon nanotubes, the interaction with EVA(27) is weak; hence the effect on segmental mobility and crystallization kinetics is negligible. In case of polar Cloisite[®] 30B clay, the interaction with the vinyl acetate units in EVA(27) is strong but limited to the amorphous fraction of the matrix. Therefore, its influence on the crystallinity of the matrix is limited, even though the upward shift in the melting temperature might be indicative for the occurrence of some interaction with the crystallizable segments as well [also observed for EVA(19), Fig. 8]. On the other hand, a considerable decrease in the degree of crystallinity is observed for nanocomposites based on HDPE-coated carbon nanotubes and nonpolar Cloisite[®] 20A clay. This is explained by the fact that the latter nanofillers directly interact with the crystallizable ethylene segments of EVA, therefore strongly influencing their crystallization. These observations further support the above discussion on the effect of interaction type and segmental mobility issues on the magnitude of C_p^{excess} during quasi-isothermal crystallization.

Finally, it is worth noting that the HDPE coating around the carbon nanotubes is highly crystalline and shows a prominent melting transition at about $130\text{ }^{\circ}\text{C}$ (Fig. 9). Furthermore, the poly(ethylene) is still able to undergo crystal annealing, as demonstrated by the particular melting behavior of a sample annealed at $130\text{ }^{\circ}\text{C}$. Since crystal reorganization during an annealing step requires a

certain degree of mobility of the polymer chains, this provides additional evidence for the weak interaction between the carbon nanotubes and HDPE or ethylene segments of EVA, in line with the observations from quasi-isothermal crystallization, that is, EVA in contact with nontreated carbon nanotubes.

CONCLUSIONS

Melt mixing has been used for the preparation of nanocomposites based on HDPE or various types of EVA copolymer, in combination with several types of organoclay or carbon nanotubes. Our main concern was to investigate the interplay between matrix and filler polarities, and to gain insight into how this affects the matrix-filler interaction in these nanocomposites. Along with a proper dispersion quality of the nanofiller, which determines the amount of matrix-filler interface available for interaction, the type and strength of interaction is one of the key parameters for achieving the intended property enhancements. A novel methodology using MTDSC was presented to assess the latter interaction strength. The sample morphology and dispersion quality of the nanofillers were evaluated using AFM; MTDSC was used to investigate the thermal properties of the nanocomposites.

It was shown that during quasi-isothermal crystallization an excess contribution is observed in the MTDSC heat capacity signal, which is due to reversible melting and crystallization of part of the matrix polymer on the timescale of the imposed temperature modulation. In case of a polar matrix, its magnitude is strongly reduced upon addition of organoclay, whereas it remains unchanged when carbon nanotubes are incorporated into the matrix polymer. Functionalization of these nanotubes or surrounding them by a polymer coating, however, does lead to a decrease in the magnitude of the excess heat capacity, suggesting that it is related to the occurrence of specific matrix-filler interactions. It is therefore advanced that the magnitude of this excess contribution depends on the segmental mobility of the crystallizable polymer chains in the vicinity of the nanofiller, which is governed by the type and strength of the matrix-filler interaction. Hence, the presented methodology provides nanoscale information on phenomena occurring at the polymer-filler interface and allows investigating how polymer mobility and crystallization behavior are locally affected in the nanocompo-

sites. It was shown that untreated carbon nanotubes undergo limited interaction with the EVA matrix. Reduction in the segmental mobility of polymer chains was observed in case of polar nanofillers, but the interaction predominantly occurs with the vinyl acetate moieties located in the amorphous polymer fraction. Direct interaction with the crystalline polymer fraction occurs when nonpolar nanofillers are used, even though their interaction with the crystallizable ethylene sequences is weaker.

Finally, the peculiar melting behavior of the nanocomposites based on EVA copolymer was investigated. It is suggested that a certain degree of ordering is present in the melt, due to the segregation of a vinyl acetate rich fraction on a molecular level. This could explain the observed nucleation behavior, as attested by the absence of an induction period during quasi-isothermal crystallization. Additional crystal nucleation can be achieved by the incorporation of carbon nanotubes, either untreated or coated with HDPE.

The work of H.E. Miltner was supported by a grant of the Research Foundation Flanders (FWO-Vlaanderen). Ph. Dubois and S. Peeterbroeck acknowledge the 'Région Wallonne' for financial support in the frame of the Nanotechnology project BINANOCO. This work was partly supported by the Belgian Federal Government Office of Science Policy (SSTC-PAI 5/3). Ph. Dubois is much indebted to both 'Région Wallonne' and European Community 'FSE and FEDER' for financial support in the frame of Objectif-1 Hainaut: Materia Nova.

We thank the NMR Laboratory of Prof. J. B. Nagy at the FUNDP (Belgium) for kindly supplying all carbon nanotube samples.

REFERENCES AND NOTES

- Alexandre, M.; Dubois, P. *Mat Sci Eng R* 2000, 28, 1–63.
- Ray, S. S.; Okamoto, M. *Prog Polym Sci* 2003, 28, 1539–1641.
- Thostenson, E. T. L.; Chou, T.-W. *Compos Sci Technol* 2005, 65, 491–516.
- Velasco-Santos, C.; Martinez-Hernandez, A. L.; Castano, V. M. *Compos Interfaces* 2005, 11, 567–586.
- Tasis, D.; Tagmatarchis, N.; Bianco, A.; Prato, M. *Chem Rev* 2006, 106, 1105–1136.
- Miltner, H. E.; Van Assche, G.; Pozsgay, A.; Pukánszky, B.; Van Mele, B. *Polymer* 2006, 47, 826–835.
- Miltner, H. E.; Rahier, H.; Pozsgay, A.; Pukánszky, B.; Van Mele, B. *Compos Interfaces* 2005, 12, 787–803.

8. Vast, L.; Philippin, G.; Destree, A.; Moreau, N.; Fonseca, A.; Nagy, J. B.; Delhalle, J.; Mekhalif, Z. *Nanotechnology* 2004, 15, 781–785.
9. Peeterbroeck, S.; Lepoittevin, B.; Pollet, E.; Benali, S.; Broekaert, C.; Alexandre, M.; Bonduel, D.; Viville, P.; Lazzaroni, R.; Dubois, P. *Polym Eng Sci* 2006, 46, 1022–1030.
10. Reading, M.; Luget, A.; Wilson, R. *Thermochim Acta* 1994, 238, 295–307.
11. Wunderlich, B.; Jin, Y.; Boller, A. *Thermochim Acta* 1994, 238, 277–293.
12. Ishikiriya, K.; Wunderlich, B. *J Polym Sci Part B: Polym Phys* 1997, 35, 1877–1886.
13. Minakov, A. A.; Schick, C. *Thermochim Acta* 1999, 330, 109–119.
14. Scherrenberg, R.; Mathot, V.; Van Hemelrijck, A. *Thermochim Acta* 1999, 330, 3–19.
15. Dreezen, G.; Groeninckx, G.; Swier, S.; Van Mele, B. *Polymer* 2001, 42, 1449–1459.
16. Swier, S.; Pieters, R.; Van Mele, B. *Polymer* 2002, 43, 3611–3620.
17. Swier, S.; Van Durme, K.; Van Mele, B. *J Polym Sci Part B: Polym Phys* 2003, 41, 1824–1836.
18. Van Durme, K.; Verbrugge, S.; Du Prez, F.; Van Mele, B. *Macromolecules* 2004, 37, 1054–1061.
19. Van Durme, K.; Van Assche, G.; Van Mele, B. *Macromolecules* 2004, 37, 9596–9605.
20. Pyda, M., Ed. *ATHAS databank*; Available at <http://athas.prz.edu.pl/databank/intro.html>.
21. Mainil, M.; Alexandre, M.; Monteverde, F.; Dubois, P. *J Nanosci Nanotechnol* 2006, 6, 337–344.
22. Vaia, R. A.; Giannelis, E. P. *Macromolecules* 1997, 30, 7990–7999.
23. Bugada, D. C.; Rudin, A. *Eur Polym Mater* 1992, 28, 219–227.
24. Alexandre, M.; Beyer, G.; Henrist, C.; Cloots, R.; Rulmont, A.; Jérôme, R.; Dubois, P. *Macromol Rapid Commun* 2001, 22, 643–646.
25. Jeon, C. H.; Ryu, S. G.; Chang, Y.-W. *Polym Int* 2003, 52, 153–157.
26. Chaudhary, D. S.; Prasad, R.; Gupta, R. K.; Bhattacharya, S. N. *Polym Eng Sci* 2005, 45, 889–897.
27. Zhang, F.; Sundararaj, U. *Polym Compos* 2004, 25, 535–542.
28. Gelfer, M.; Song, H. H.; Liu, L.; Avila-Orta, C.; Yang, L.; Si, M.; Hsiao, B. S.; Chu, B.; Rafailovich, M.; Tsou, A. H. *Polym Eng Sci* 2002, 42, 1841–1851.
29. Gelfer, M. Y.; Burger, C.; Chu, B.; Hsiao, B. S.; Drozdov, A. D.; Si, M.; Rafailovich, M.; Sauer, B. B.; Gilman, J. W. *Macromolecules* 2005, 38, 3765–3775.
30. Su, Z.; Zhao, Y.; Xu, Y.; Zhang, X.; Zhu, S.; Wang, D.; Wu, J.; Han, C. C.; Xu, D. *Polymer* 2004, 45, 3693–3700.
31. Li, S.-N.; Li, Z.-M.; Yang, M.-B.; Hu, Z.-Q.; Xu, X.-B.; Huang, R. *Mater Lett* 2004, 58, 3967–3970.
32. Moly, K. A.; Bhagawan, S. S.; Groeninckx, G.; Thomas, S. *J Appl Polym Sci* 2006, 100, 4526–4538.
33. John, B.; Varughese, K. T.; Oommen, Z.; Pötschke, P.; Thomas, S. *J Appl Polym Sci* 2003, 87, 2083–2099.
34. Khonakdar, H. A.; Wagenknecht, U.; Jafari, S. H.; Hässler, R.; Eslami, H. *Adv Polym Technol* 2004, 23, 307–315.
35. Zhang, Q.; Lin, W.; Yang, G.; Chen, Q. *J Polym Sci Part B: Polym Phys* 2002, 40, 2199–2207.